Design of a real-time two-color interferometer for MAST Upgrade

O'Gorman T, Naylor G, Scannell R, Cunningham G, Brunner K J, Martin R, Croft D

AIP | Review of Scientific Instruments

Design of a real-time two-color interferometer for MAST Upgradea)

T. O'Gorman, G. Naylor, R. Scannell, G. Cunningham, K. J. Brunner, R. Martin, and D. Croft

Citation: Review of Scientific Instruments **85**, 11D861 (2014); doi: 10.1063/1.4894394
View online: http://dx.doi.org/10.1063/1.4894394
View Table of Contents: http://scitation.aip.org/content/aip/journal/rsi/85/11?ver=pdfcov
Published by the AIP Publishing

Design of a real-time two-color interferometer for MAST Upgrade[a)]

T. O'Gorman,[1,b)] G. Naylor,[1] R. Scannell,[1] G. Cunningham,[1] K. J. Brunner,[2] R. Martin,[1] and D. Croft[1]
[1]*CCFE, Culham Science Centre, Abingdon, Oxon OX14 3DB, United Kingdom*
[2]*Centre for Advanced Instrumentation, Department of Physics, Durham University, DH1 3LE, United Kingdom*

(Presented 2 June 2014; received 31 May 2014; accepted 13 August 2014; published online 17 September 2014)

A single chord two-color CO_2/HeNe (10.6/0.633 μm) heterodyne laser interferometer has been designed to measure the line integral electron density along the mid-plane of the MAST Upgrade tokamak, with a typical error of 1×10^{18} m^{-3} ($\sim 2^\circ$ phase error) at 4 MHz temporal resolution. To ensure this diagnostic system can be restored from any failures without stopping MAST Upgrade operations, it has been located outside of the machine area. The final design and initial testing of this system, including details of the optics, vibration isolation, and a novel phase detection scheme are discussed in this paper. [http://dx.doi.org/10.1063/1.4894394]

I. INTRODUCTION

Electron density (n_e) is an important parameter to measure on tokamak plasmas and enables plasma control. Two-color interferometers are employed on a number of tokamaks[1–3] to make n_e measurements integrated along a particular line of sight ($\int n_e dl$) using two superimposed laser interferometers with different wavelengths (λ). Two interferometers are needed in order to distinguish between phase changes resulting from $\int n_e dl$ and those arising from vibrations (Δl) of the optical components. A new two-color interferometer has been developed for MAST Upgrade (MAST-U)[4] that consists of both CO_2 ($\lambda_C = 10.6$ μm) and HeNe ($\lambda_H = 0.633$ μm) laser interferometers, with a single chord traversing the mid-plane of the MAST-U vessel with a tangency of 0.3 m to the center column (see Fig. 1). The phase change for each interferometer $\theta_{C,H}$ is given by

$$\theta_{C,H} = 2.82 \times 10^{-15} \lambda_{C,H} \int n_e dl + \frac{2\pi \Delta l}{\lambda_{C,H}}. \quad (1)$$

As λ_H is shorter than λ_C the HeNe interferometer is more sensitive to vibrations, while the CO_2 interferometer is more sensitive to $\int n_e dl$. Rearranging Eq. (1) allows $\int n_e dl$ to be expressed independent of Δl, and instead in terms of the difference in the phase measurements of the HeNe and CO_2 interferometers,

$$\int n_e dl = \frac{\theta_C - (\lambda_H/\lambda_C)\theta_H}{2.82 \times 10^{-15} \lambda_C (1 - (\lambda_H/\lambda_C)^2)}. \quad (2)$$

Although this new system is closely based on the previous MAST interferometer[5] in terms of the choice of lasers and the position of the single chord traversing the MAST vessel, key changes have been made in order to improve both the temporal resolution and the availability and reliability of the system. First, the temporal resolution of the previous system was limited to 50 kHz. However, higher temporal resolution measurements are needed for the study of a number of tokamak instabilities which evolve on microsecond timescales, such as edge localized modes[6] and toroidal Alfven eigenmodes.[7] A new field programmable gate array (FPGA) based phase detection system has therefore been developed for the new system and allows a temporal resolution of 4 MHz. Second, the previous interferometer system was located inside the MAST vessel area, which restricted access during operations and affected reliability when high energy X-rays were generated. System reliability is important as its measurements will be used for real-time plasma feedback control and in the new system reliability is improved by locating the majority of components outside of the MAST-U vessel area. This will also allow access during operations.

In Secs. II–V, the optical design, phase detection, anti-vibration hardware, and initial testing of the new interferometer system will be discussed in more detail.

II. OPTICAL DESIGN

The CO_2 laser is a waveguide, water cooled 8W Merit SL from Access Lasers, which has a coherence length of >1 m. The important parameters for both the CO_2 and HeNe lasers are shown in Table I.

The optical path of the CO_2 interferometer is shown in Fig. 2. Due to the large divergence (see Table I) of the CO_2 laser, an f = 0.5 m ZnSe lens ($L1$, Fig. 2) is used to reduce the beam waist to match the aperture of the acousto-optic modulator (AOM), which splits the CO_2 laser into a scene beam (dotted black line, Fig. 2) and a 40 MHz frequency shifted reference beam (solid blue line). Both scene and reference beams are then collimated by telescopes, which incorporate an f = −100 mm lens (L2, Fig. 2) and f = 762 mm mirrors (M1), to ensure that the beam radius (1/e in amplitude) is less than 7.5 mm at the input and output windows of the vessel and 5 mm at the in-area retro reflector (RR3).

To facilitate easy realignment of the system if needed, HeNe and CO_2 beam combiners (BC, Fig. 2) are used to overlay HeNe alignment beams on both the scene and reference beams. The scene beam then travels out through the MAST-U

[a)]Contributed paper, published as part of the Proceedings of the 20th Topical Conference on High-Temperature Plasma Diagnostics, Atlanta, Georgia, USA, June 2014.
[b)]Electronic mail: thomas.ogorman@ccfe.ac.uk

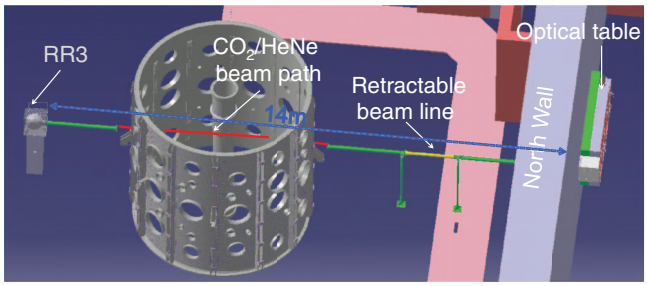

FIG. 1. Layout of interferometer system on MAST-U. The optical bench is mounted on the north wall. Lasers are directed through a mid-plane port of the MAST-U vessel, exit a port at the other side of the vessel, and are reflected back from the in-area retro reflector (RR3). The distance from the optical bench to the RR3 is 14 m.

vessel to RR3 and back to a 50:50 beam splitter. To match the distance traveled by the scene beam, the reference beam is directed onto two folding mirrors (M2 and M3, Fig. 2), for 14 bounces of 1.8 m each, before also being directed to the beam splitter where it interferes with the scene beam. The signal from the beam splitter is focused onto the detector using a mirror (M4, Fig. 2) and the interference fringes measured.

The optical path of the HeNe interferometer is shown in Fig. 2 (dotted red line). An Agilent 5517B HeNe laser produces two superimposed orthogonally polarized beams with a frequency difference of ∼ 2.3 MHz. A polarization-dependent beam splitter (PBS, Fig. 2) separates the two beams into the scene and reference arms. The scene beam is guided though the MAST-U vessel to RR3 and back to the same beam splitter. The long coherence length of the HeNe laser means that the distance traveled by the reference beam need not match that of the scene beam. A quarter wave plate (QWP, Fig. 2) is then used in conjunction with a retro reflector (RR2, Fig. 2) to match the polarization of the reference beam to the returning scene beam, causing them to interfere. This signal is then focused onto the detector and the interference fringes measured.

III. DETECTORS AND FPGA PROCESSING

The interference signal from the CO_2 interferometer is measured on a VIGO PVM-10.6 photovoltaic detector. This signal is then amplified and passed through a Mini-Circuits 35-49 MHz bandpass filter to reduce broadband noise before it enters the phase processing unit. The HeNe interference signal is measured on a Thorlabs PDA8A silicon amplified detector. The reference signal for the CO_2 interferometer comes from the RF generator of the AOM. The phase changes of the CO_2 and HeNe interferometers are determined using an open source hardware SPEC FPGA board.[9] The logic of the FPGA firmware (used to determine the phase for each interferometer) is shown in Fig. 3.

TABLE I. Laser parameters for the CO_2 and HeNe interferometers. The beam radius and divergence are quoted at the laser outputs. M^2 is the beam quality factor.[8]

	Beam radius (mm)	Divergence (mrad)	M^2	Power stability (%)	Wavelength stability
CO_2	2.4	5.5	≤1.1	±1	$2 \times 10^{-6}\lambda_C$
HeNe	6	0.15	≤1.1	≪1	$2 \times 10^{-9}\lambda_H$

The 40 MHz CO_2 and 2.3 MHz HeNe interference and reference signals (shown as IS and Ref, respectively, in Fig. 3) are sampled at 100 MS/s using an open source hardware 14 bit digitizer.[9] The CO_2 and HeNe signals are then down-converted to ∼3.6 MHz and ∼700 kHz, respectively, by mixing them with synthetic waveforms (SIN and COS), which are generated on the FPGA to produce the I and Q quadrature components of each input signal. The signals are then 4-fold decimated to 20 MS/s and evaluated using the coordinate rotation digital computer (CORDIC) algorithm[10] to determine the phase and amplitude of each channel. The CORDIC outputs are then transmitted over an optical fiber to a PC, or processed on the FPGA and sent to the MAST-U plasma control system.

Initial measurements suggest that the phase error of the FPGA detection system is only 1°, a factor of 3 lower than the phase error of the previous MAST detection system. In addition, the new system can provide phase measurements at 20 MS/s, compared to 100 kS/s for the previous MAST interferometer. Maximum temporal resolutions are 4 MHz and 1 MHz for the CO_2 and HeNe interferometers, respectively.

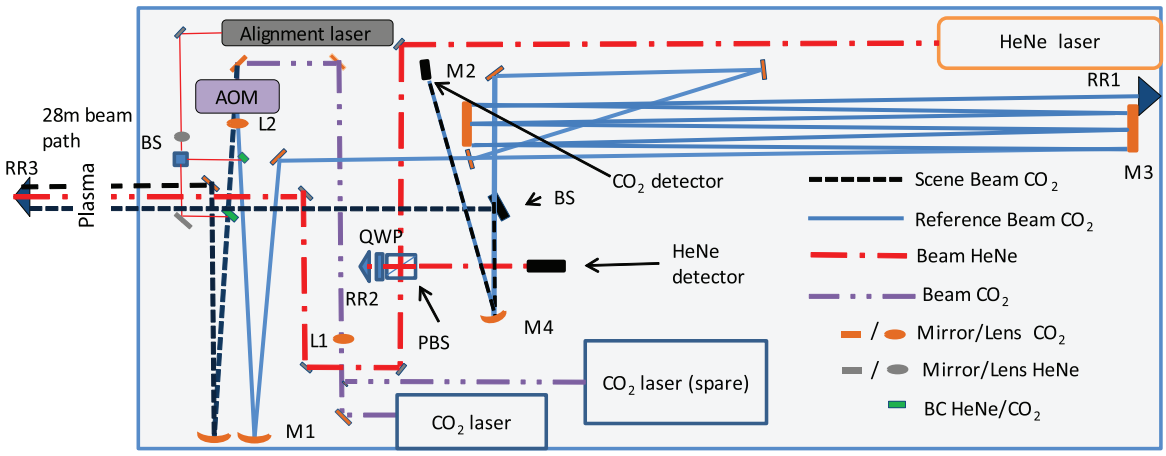

FIG. 2. A schematic of the optical layout of the MAST interferometer. BS, PBS, BC, QWP, and RR refer to beam splitter, polarizing beam splitter, beam combiner, quarter wave plate, and retro reflector, respectively. M1, M2, M3, and M4 refer to mirrors and L1 and L2 refer to lenses, all of which are referenced in the text. A spare CO_2 laser is shown, which can be employed if needed using a flip-in mirror.

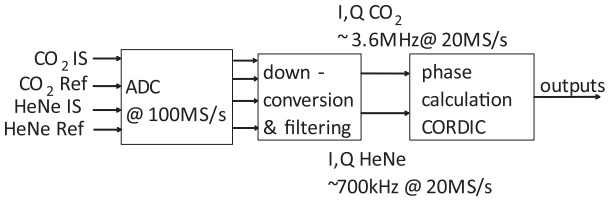

FIG. 3. The logic of the FPGA firmware used for the phase detection. This has been divided into three major processing blocks and the sampling rate for each is shown in units of MS/s.

IV. ANTI-VIBRATION HARDWARE

RR3 is located next to the neutral beam injector and the MAST-U vessel, both of which are likely to be sources of vibrations. In order to isolate RR3 from vibrations, it is mounted on an ~80 kg granite sphere, which in turn is mounted upon 3 air vibration-isolation mounts. The pressure of these isolation mounts is controlled by regulated pressure valves connected to the MAST-U air supply. They have a low natural resonant frequency of 3.5 Hz and are designed to dampen vibrations at all frequencies above this. Finally, the optical bench is designed to dampen vibrations and anti-vibration pads will be inserted between the bench and the north wall for further vibration dampening.

V. TESTING

The system cannot be installed on MAST-U until the vessel has been reassembled and moved back into the machine area. It has, however, been assembled for testing. The testing layout is similar to that planned for MAST-U except for the following variations. First, the optical table is mounted horizontally instead of vertically on a wall. Second, the scene arm has been propagated on a set of folding mirrors located on the optical bench and finally, the phase measurements were performed using the real-time phase processing electronics from the previous MAST interferometer, as the FPGA system is currently being commissioned.

System tests show that the measured CO_2 and HeNe fringe peak-peak amplitudes are both 50% of the DC amplitude. The fringe amplitude limit for CO_2 is set by the damage threshold of the CO_2 detector, which limits the power on the detector to 1 W. The power levels of the scene and reference beams are similar in magnitude and this enables the interference signal to be maximized. The coherency length of the CO_2 laser has been measured as >1 m by scanning the length of the scene arm and monitoring the magnitude of the interference fringes. The alignment of both interferometers has been found to be stable over a number of days' testing and the HeNe alignment beam allows quick adjustment of the CO_2 interferometer alignment if any misalignment does occur. Finally, measurements of the beam waist at a number of points along the laser path have shown values which are in agreement with Gaussian beam propagation estimates.

To test the performance of the CO_2 and HeNe interferometers in the absence of a plasma, a 10 W vibration speaker was used to induce vibrations at the location of RR3 (Fig. 2).

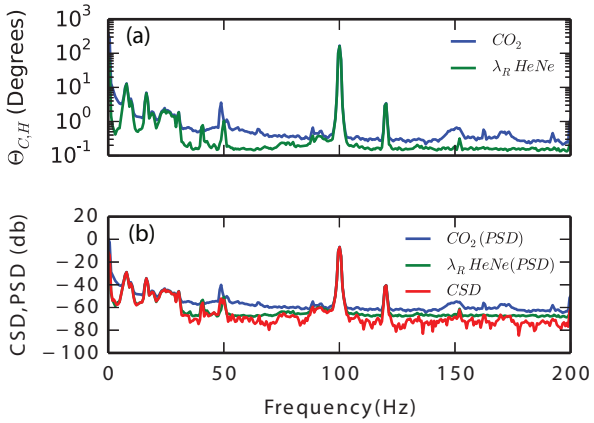

FIG. 4. (a) Phase changes for the HeNe and CO_2 interferometers. The amplitudes of the HeNe phase have been scaled by ($\lambda_R = \lambda_H/\lambda_C$). (b) Cross spectral density (CSD) and power spectral density (PSD) of phase signals from the CO_2 and HeNe interferometers.

Fig. 4 shows the change in phase at a given frequency as measured by the phase processing electronics of the previous MAST interferometer over 100 s. The HeNe phase has been scaled by the ratio between the wavelengths ($\lambda_R = \lambda_H/\lambda_C$) so that a vibration will result in a similar phase change in both interferometers. Both interferometers measure a similar frequency spectrum, which is dominated by 100 Hz, 5 μm vibrations and an additional 120 Hz, 1.5 μm harmonic which is driven by the vibration speaker at RR3 (Fig. 4(a)). The power spectral density shared by both interferometer vibration signals can be determined using the cross-spectral density of their signals and once again, there is a good match to the power spectral density of both signals (Fig. 4(b)).

Initial results from testing the new MAST-U interferometer are encouraging. Future work will involve testing the long term stability of the system, in particular, the wavelength and power stability of the CO_2 lasers. The FPGA phase detection system also needs benchmarking against the previous MAST system. The completed system will be installed on MAST-U when the vessel is moved back into the machine area.

ACKNOWLEDGMENTS

This work was part-funded by the RCUK Energy Programme [Grant No. EP/I501045] and by the European Union's (EU) Horizon 2020 research and innovation programme. To obtain further information on the data and models underlying this paper please contact PublicationsManager@ccfe.ac.uk. The views and opinions expressed herein do not necessarily reflect those of the European Commission.

[1]D. R. Baker and S. T. Lee, Rev. Sci. Instrum. **49**, 919 (1978).
[2]T. N. Carlstrom, Rev. Sci. Instrum. **59**, 1063 (1988).
[3]M. A. Van Zeeland, Rev. Sci. Instrum. **84**, 043501 (2013).
[4]W. Morris, IEEE Trans. Plasma Sci. **42**, 402 (2014).
[5]G. Cunningham, ST Workshop, Seattle, 1995.
[6]R. Scannell, Plasma Phys. Controlled Fusion **49**, 1431 (2007).
[7]M. A. Van Zeeland and G. J. Kramer, AIP Conf. Proc. **988**, 103 (2008).
[8]A. E. Siegman, Proc. SPIE **1868**, 2 (1993).
[9]See http://www.ohwr.org/projects/spec/wiki for information about the SPEC FPGA board.
[10]J. S. Walther, J. VLSI Signal Process. Syst. **25**, 107 (2000).